Ductile deformation of core-shell Si-SiC nanoparticles controlled by shell thickness

Dimitrios Kilymis, Céline Gérard, Laurent Pizzagalli

Ductile deformation of core-shell Si–SiC nanoparticles controlled by shell thickness

D. Kilymis[a], C. Gérard[a], L. Pizzagalli[a,*]

[a]*Institut Pprime - CNRS UPR3346, Université de Poitiers - CNRS - ISAE-ENSMA, F86962 Chasseneuil Futuroscope Cedex, France*

Abstract

Although the literature on mechanical properties of nanostructures is extensive, there are still few studies focusing on core–shell nanoparticles. In these systems, which are interesting in a broad range of applications, one could genuinely assume that the softest part, be it the core or the shell, will first yield when submitted to compression. To test this view, we have carried out large scale molecular dynamics simulations of uniaxially compressed core–shell Si–SiC nanoparticles. Our first conclusion is that for the investigated size range (diameters equal or below 50 nm), the nanoparticles yield plastically with no signs of fracture, in agreement with experiments on single material systems. Furthermore, our investigations also reveal that depending on the shell thickness, plastic deformation is confined either in the core or in the shell. We propose a model, based on the theory of contact mechanics and geometrical arguments, to explain this surprising result. Furthermore, we find that for a specific shell to diameter ratio, corresponding to the transition between core and shell, the stress concentration in the nanoparticles is apparently hindered, leading to a delayed plastic deformation.

Keywords: Core–shell; Plasticity; Dislocations; Silicon; Silicon Carbide

1. Introduction

Among nanostructured materials, core–shell nanoparticles begin to attract widespread interest because of promising prospects in nanotechnology, nanoelectronics, nanocatalysis, optics, nanomedicine, energy storage, or nanobiology [1, 2]. Compared to nanoparticles made of a single material, these systems offer additional advantages such as synergistic or enhanced properties coming from the interaction between core and shell, while preserving the high surface-to-volume ratio. Furthermore, the core–shell interface can also be a key tunable parameter, increasing even more capabilities.

All these aspects motivated an exponentially growing number of studies aiming at a better understanding and control of the features of core–shell nanoparticles. However, the focus is usually put on optical, electronic or catalytic aspects, but rarely on mechanical properties. Our knowledge regarding how core–shell nanoparticles would respond to a mechanical sollicitation is still in its infancy. For systems with one or several nanometric dimensions, it is now well established that mechanical properties can be greatly modified compared to bulk materials, mainly because of the presence of surfaces [3, 4]. This is often coined as a size effect, as dimension reduction tends to increase the surface-to-volume ratio. In core–shell systems, the influence of surfaces is also expected, but the presence of two different materials, and the interface in between, could further significantly change mechanical properties.

In the literature, most of the relevant information on the mechanical properties actually concerns systems with a shell harder than the core [5]. For instance, spectacular shape restoration effects were discovered for silica coated silver nanowires [6], and for a-Si coated aluminum nanodots [7]. Recently, Godet et al. showed that a quasi-perfect elasto-plastic regime could be reached during the tensile deformation of a-Si coated gold nanowires [8]. These few results suggest that original and unforeseen behaviors could be expected for core–shell nanoparticles.

In this paper we describe our theoretical investigations of the mechanical properties of core–shell Si–SiC nanoparticles. These systems are chosen for the following reasons. On the one hand, silicon is a model for covalent materials, and its bulk plasticity properties are reasonably known [9]. Furthermore, we have at our disposal an abundant information on the mechanical properties of silicon nanoparticles [10–14]. On the other hand, Si–SiC composites are promising materials for sensors in bionanotechnology [15], because of the excellent biocompatibility and functionalization capability of silicon carbide, while silicon remains the base material in current electronic devices. Moreover spherical Si–SiC nanoparticles are experimentally feasible systems, since several synthesis methods have been successfully tested [16–18].

Our investigations bring several important highlights. First, high applied stresses can be reached with no signs of fracture, revealing original plasticity mechanisms. Secondly, we show that the mechanical response of the Si–SiC nanoparticle is critically dependent on the shell thickness, with a plastic deformation either confined in the SiC shell or in the Si core. Finally, it is revealed that at the transition, stress concentration is apparently inhibited, yielding an original and unprecedented elastic state at the onset of plastic deformation.

*Corresponding author

Email address: laurent.pizzagalli@univ-poitiers.fr (L. Pizzagalli)

2. Models and methods

Table 1: Diameter $\varnothing$ and shell thickness δ parameters (in nm) for the nanoparticle configurations investigated in this work.

$\varnothing$ (nm)	SiC shell thickness δ (nm)
50	0 (Si NP) / 2.5 / 5.0 / 8.8 / 12.5 / 25.0 (SiC NP)
20	0 (Si NP) / 1.0 / 2.0 / 3.5 / 5.0 / 10.0 (SiC NP)

Several models of spherical Si–SiC core–shell nanoparticle are studied in this work. They are built by first carving spheres of diameter $\varnothing$ from a perfect silicon crystal of lattice parameter equal to 5.43 Å. Then the region defined by a spherical shell starting from the surface and of width δ is emptied and next filled by a cubic silicon carbide crystal of lattice parameter equal to 4.36 Å, with the same orientation than the remaining silicon part. This procedure creates a Si–SiC core–shell nanoparticle with an unrelaxed sharp and incoherent interface (Fig. 1-a). In a second step, a NVT molecular dynamics run of 70 ps and at a temperature of 300 K is performed to improve the interface quality. This defines the core–shell nanoparticles with a 'sharp' Si/SiC interface. Two different nanoparticles sizes, with $\varnothing$ = 20 nm, 50 nm, and several shell thicknesses are studied (Table 1). We also consider pure Si and SiC nanoparticles, in order to compare with core–shell systems.

A second set of configurations with a 50 nm diameter and a different Si/SiC interfacial structure has been generated. Starting from a system with an unrelaxed sharp interface, a shell part of the Si core is replaced with a disordered SiC phase including $^2/_3$ Si and $^1/_3$ C. This composition corresponds to the volumetric mixing of 50% of Si and SiC, when the lattice parameter differences between Si and SiC is taken into account. Starting from the Si/SiC boundary, and for a thickness 2.5 nm, Si and C atoms are randomly placed in cubic diamond lattice positions, defined with a lattice constant of 4.90 Å equal to the average of Si and SiC lattice constants. The whole system is then first relaxed with conjugate gradient. Next, a NVT molecular dynamics run of 200 ps and at a temperature of 300 K is carried out. We find that this procedure allows for obtaining a mechanically and structurally stable amorphous interface (Fig. 1-b). Additional calculations made with longer durations and higher temperatures do not bring significant changes. The respective widths of 'sharp' and 'amorphous' interfaces can be seen in the Figure 1-c.

The LAMMPS package [19, 20] is used to perform all molecular dynamics and conjugate gradient simulations. The integration of the equation of motions is done with a timestep of 1 fs, and temperature is controlled using a Nose-Hoover thermostat. Uniaxial compression is achieved by using two moving virtual planar indenters, defined by a quadratic repulsive force field as implemented in LAMMPS [21]. Infinitely hard indenters are set using a force field parameter equal to 1000 eV Å^{-3} [14, 22]. These indenters are initially located on each side of the nanoparticle, and move towards each other at a constant velocity of 0.1 Å/ps during compression tests, with a $\langle 100 \rangle$ orientation relatively to the silicon lattice. This corresponds to engineering strain rates of 2×10^8 s^{-1} (5×10^8 s^{-1}) for a $\varnothing$ = 50 nm ($\varnothing$ = 20 nm) nanoparticle, which is typical of molecular dynamics simulations. Interatomic interactions are described using the environment-dependent interatomic potential (EDIP) [23], with parameters specifically generated for an accurate description of extended defects in both silicon and silicon carbide [24]. All simulations are carried out at both 5 K and 300 K, to investigate a possible influence of temperature on plasticity mechanisms.

To determine the true compression stress, it is necessary to estimate the contact surface area between the indenter and the nanoparticle. It is determined by first finding atoms distant from the indenter by less than 1 Å. Next, the contact surface area can be estimated by a Delaunay triangulation of these atom positions. Although the distance criterion used here is arbitrary, we find that reasonable increase or decrease of this threshold lead to negligible differences in contact surface area. Finally, the true stress is calculated as the ratio between the response force acting on one indenter and the contact surface area.

Finally, during molecular dynamics simulations, the atomic stress tensors for each atom i (of mass m_i) are calculated using the Virial theorem:

$$\sigma_{\alpha\beta} = -\frac{1}{V_i}\left[\frac{1}{2}\sum_{j=1}^{N} x_\alpha^j f_\beta^j + \mathrm{m}^i v_\alpha^i v_\beta^i\right] \tag{1}$$

where x_α^j, v_α^j are the positions and velocities of all neighboring atoms along the α direction, while f_β^j is the force they exert on the atom i (of mass m_i) along the β direction. The atomic volumes V_i is calculated using the Voronoi tessellation method. Since the latter quantity is ill defined for surface atoms, atomic stresses are used only for non-surface atoms.

The atomic stress tensors are then used to compute the von Mises stresses defined as

$$\begin{aligned}\sigma^{vm} &= \frac{1}{\sqrt{2}}\Big[\left(\sigma_{xx}-\sigma_{yy}\right)^2 + \left(\sigma_{yy}-\sigma_{zz}\right)^2 + \left(\sigma_{zz}-\sigma_{xx}\right)^2 \\ &\quad + 6\left(\sigma_{xy}^2+\sigma_{xz}^2+\sigma_{yz}^2\right)\Big]^{1/2}\end{aligned} \tag{2}$$

and the hydrostatic stresses as

$$\sigma^h = \frac{1}{\sqrt{3}}\left(\sigma_{xx}+\sigma_{yy}+\sigma_{zz}\right) \tag{3}$$

Final values used in the paper are next obtained for each atom by averaging over all its neighbors in a sphere of radius equal to 5.7 Å.

3. Results

The influence of the SiC shell thickness on the mechanical response of a 50 nm nanoparticle with a sharp interface, compressed at 5 K, can be first analyzed from true stress–true strain curves, shown in Fig. 1-d. These curves are all characterized by

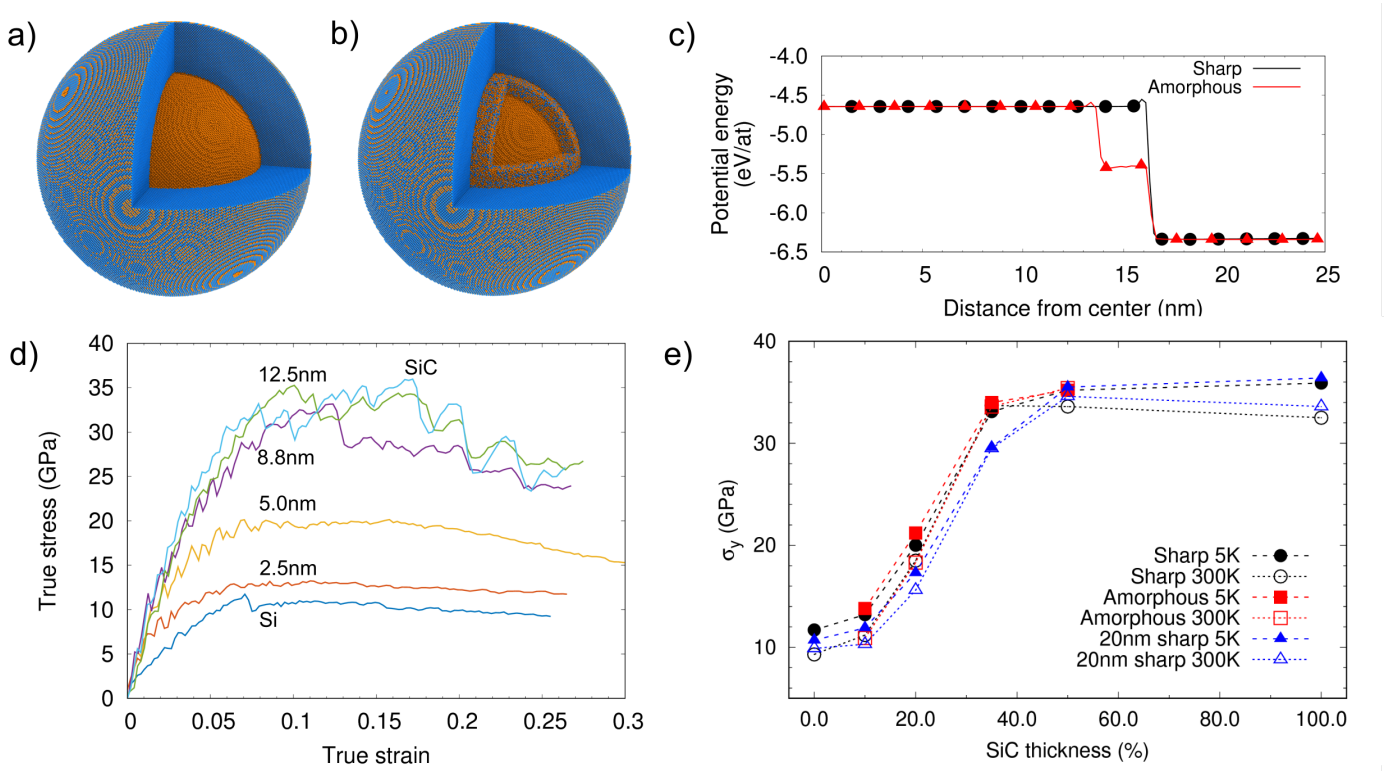

Figure 1: (a,b) Cross-section views of undeformed Si–SiC core–shell nanoparticles with a 50 nm diameter and a SiC shell thickness δ = 8.8 nm, with (a) sharp and (b) amorphous Si/SiC interfaces. (c) Average potential energy per atom from the center to the nanoparticle edge, for both (a) and (b) configurations, revealing the width of the amorphous interface structure. (d) True stress–true strain curves determined for a sharp interface 50 nm nanoparticle at 5 K, and different SiC shell thickness δ values. (e) Variation of the yield stress σ_y as a function of δ, expressed in percentage relative to the nanoparticle diameter, for different cases (circles: 50 nm sharp, squares: 50 nm amorphous, triangles: 20 nm sharp, with full symbols denoting calculations at 5 K and empty ones at 300 K).

an increase of stress at small deformation, with a mean slope approximately proportional to the SiC content. Small irregular variations are visible, which are mostly due to localized amorphization and surface reorganization, as will be discussed later. All curves saturate at a given strain, then decrease, with a particularly slow rate for nanoparticles with low SiC contents. Similar curves are obtained for other systems and different conditions.

The yield stress σ_y is here defined as the maximum stress value, as it is usually done in literature [12, 25, 26]. In Fig. 1-e σ_y is reported as a function of δ. Remarkably, a similar trend is observed for the various investigated cases: starting from a value of about 10 GPa, typical of silicon nanoparticles, σ_y quickly increases with δ, until saturation with maximum values in the range 31–36 GPa. This plateau is reached when the SiC shell thickness is about 36% of the diameter, i.e. when δ exceeds 8.8 nm. For full SiC nanoparticles compressed at 300 K, σ_y is about 31 GPa, which falls in the range of strength values reported for SiC nanostructures [27–29].

Comparing in Fig. 1-e simulations carried out at 5 K and 300 K unsurprisingly reveals that the largest σ_y values are obtained at low temperatures, since plastic deformation mechanisms in nanostructures are often thermally activated. However, the differences remain small, at most 3 GPa. A slightly more pronounced influence of size can be determined. In fact, in most cases, σ_y is greater for the 50 nm nanoparticle than for the 20 nm one, by at most 4 GPa. Full SiC systems show a reverse behavior though. Lastly, our simulations hint that the interface configuration has little effect on the nanoparticle mechanical properties. This is especially remarkable given that intuitively, one could have expected a strong dependence between mechanical yielding and the core–shell interface.

Overall the nanoparticle strength is essentially dependent on the SiC thickness. However, the shape of yield stress curves depicted in Fig. 1-e is not easy to explain. We also tried to plot σ_y as a function of the relative proportion of Si and SiC. This leads to more linear variations, but discrepancies remain, hinting that a mixing model is too simplistic to describe the strength of core-shell nanoparticles. In particular, it is noteworthy that the presence of a SiC shell with a significant thickness of 2.5 nm has little effect compared to the uncoated Si nanoparticle. Also, large σ_y values, close to the one for the full 50 nm SiC nanoparticle, are obtained when δ is only 8.8 nm.

Further information can be gained from a meticulous analysis of atomic displacements during compression tests. First, we observe that the first plastic deformation stages actually correspond to the flattening of the nanoparticle at the contact with the two virtual indenters, resulting in a localized surface amorphization. This process is repeated intermittently, leading to the irregular variations observed in the initial increasing part of stress–strain curves (Fig. 1). It is then worth mentioning that σ_y in Fig. 1-e does not always correspond to the onset of plastic

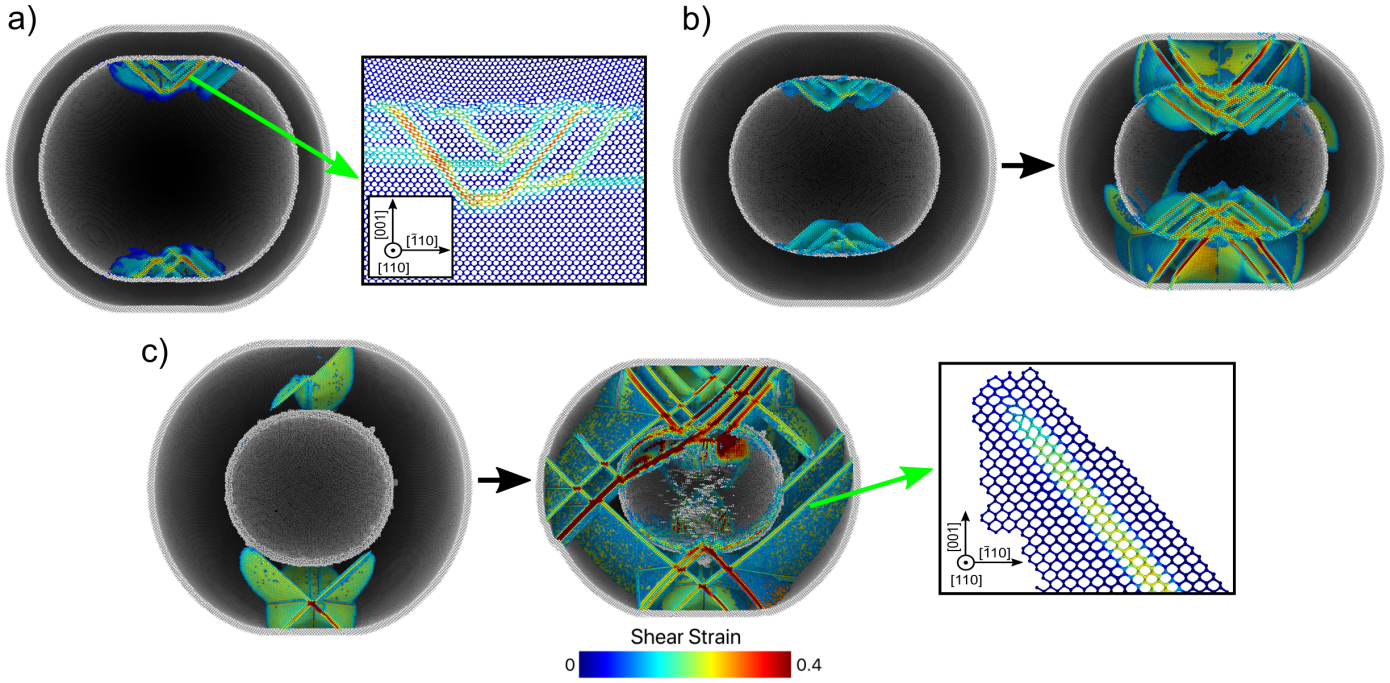

Figure 2: Cross-section views of compressed nanoparticles with a sharp Si–SiC interface and three SiC shell thicknesses δ: a) δ = 5.0 nm, temperature of 5 K, true strain ε = 0.11, b) δ = 8.8 nm, 5 K, ε = 0.12 (left) then ε = 0.20 (right), c) δ = 12.5 nm, 300 K, ε = 0.09 (left) then ε = 0.18 (right). For clarity, perfect crystal atoms inside the nanoparticle are not shown. Other atoms are colored according to the computed von Mises shear strain [30]. The two frames show slices of enlarged regions, to better visualize the structure of dislocation cores in Si and SiC, respectively.

deformation in the nanoparticles.

After this initial surface disordering, different scenarios are possible according to the SiC thickness only, with no influence of size (50 nm and 20 nm) and temperature (5 K and 300 K). For thin shells, more precisely when $\delta \leq 5.0$ nm, dislocations nucleate from the Si–SiC interface and propagate in the silicon core once a strain threshold is attained (Fig. 2-a). The latter is in most cases lower than the strain corresponding to σ_y. Dislocation nucleation is probably facilitated by the presence of atomic disorder at the interface [31]. Analysis of atomic displacements reveals that these dislocations are characterized by a Burgers vector equal to $1/6\langle 112\rangle$, i.e. they are partial dislocations, and slip in $\{111\}$ shuffle planes (Fig. 2-a). The activation of this plasticity mechanism is unexpected [32], because the $\{111\}$ shuffle stacking fault has been predicted to be unstable [33]. However, it appears that the large pressure exerted by the indenters, and transmitted to the silicon core by the thin SiC shell, is sufficient to make it stable. The same mechanism is observed for pure Si nanoparticles, with the nucleation of partial dislocations from the partially amorphized contact surface. Note that it is now well documented that the plastic deformation along $\langle 100\rangle$ of silicon nanospheres is critically dependent on the choice of the interatomic potential in molecular dynamics simulations. For instance, with the Tersoff potential [34], a β-tin phase transformation is observed, whereas Stillinger-Weber potentials result in the nucleation of perfect $1/2\langle 110\rangle$ dislocations [14, 25, 35]. To gain further insights, we performed additional calculations using the Erhart-Albe SiC potential [36] as an alternative to EDIP. Interestingly, the nucleation of shuffle partial dislocations is also observed with this potential.

The partial dislocations propagate slowly during compression, like punched dislocation loops, essentially pushed by the applied load, and thus relaxing a limited amount of stress. This explains why there are no sharp stress decreases on stress–strain curves, due to the lack of avalanches of fast-moving dislocations, and also why the nucleation of the first dislocations occurs before σ_y is reached.

These partial dislocations are nucleated in the four equivalent $\{111\}$ slip systems, at different interface locations, thus forming several inversed pyramidal structures below or above the indenters (Fig. 2-a). For large deformations, additional dislocations can nucleate from the edges of these structures. The whole process is very similar to what is observed during the $\langle 100\rangle$ compression of metallic nanospheres [22]. Finally, we stress that the plastic deformation remains confined into the silicon core, even for large plastic deformation.

In the case of thick SiC shells, i.e. $\delta \geq 12.5$ nm, plastic deformation proceeds according to a different scenario: half-loop dislocations with Burgers vector equal to $1/2\langle 110\rangle$ nucleate in the vicinity of the surfaces in contact with indenters, and propagate in shuffle $\{111\}$ planes (Fig. 2-c). The leading edge exhibits a 60° character, with a dislocation core easily recognizable (see enlarged region in Fig. 2-c), and two screw arms connected to the surface. The presence of similar perfect $\{111\}$ dislocations in SiC has been reported in experiments [37]. Increasing the load leads to nucleation of additional dislocations from the surface, or to dislocation expansion in secondary planes by cross-slip.

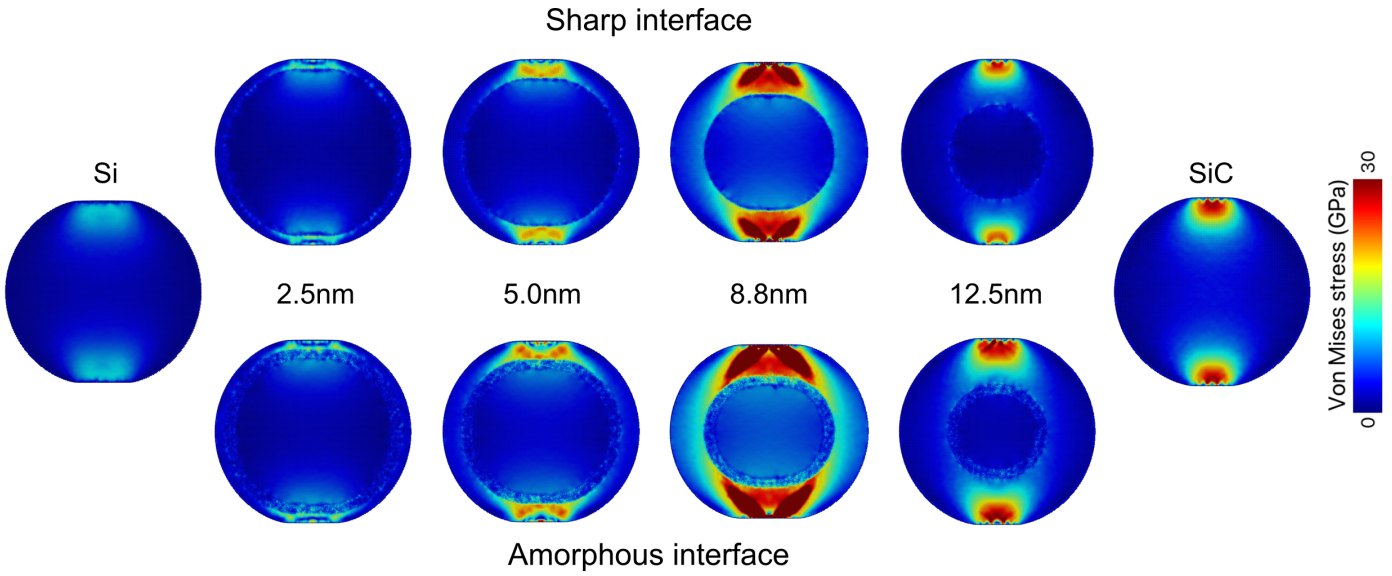

Figure 3: Cross section views of von Mises stress spatial distributions computed right before dislocations are nucleated, from compression tests of 50 nm nanoparticles at 5 K. The SiC shell thickness δ (reported in the middle of the figure) increases from the left to the right, the two extreme cases being the full Si (left) and full SiC (right) nanoparticles. Top (bottom) configurations correspond to a sharp (amorphous) interface, respectively.

Remarkably, dislocation activity remains now essentially confined in the SiC shell, even for large applied loads. Dislocations preferentially nucleate and glide in planes that do not cross the silicon core. The latter is then highly compressed but not sheared by dislocations. There are rare exceptions though, like represented in Fig. 2-c. Here, a perfect dislocation, which nucleated and terminated at the SiC shell surface, succeeds in cutting across the silicon core during its propagation at high strain.

It is also of interest to describe an additional scenario, obtained for an intermediate SiC thickness value (δ = 8.8 nm). In that case, plastic deformation first occur by the nucleation of partial dislocations from the Si–SiC interface followed by their slow migration into the silicon core (Fig. 2-b). However, at a certain strain, further dislocations nucleate from the Si–SiC interface, but they are now perfect, and migrate into the SiC shell. These dislocations seem to be somewhat connected to the nucleation sites of the primary partial dislocations, but the interface is not ordered enough to draw a clear and definite conclusion.

Finally, a common point to all the systems we investigated is the absence of fracture during deformation, even at large strains. This might be surprising, since both silicon and silicon carbide are brittle materials at the considered temperatures. Furthermore, the Si–SiC interface could be assumed to be a potential source for crack initiation. However, it is now widely recognized that the ductile deformation of brittle materials is favored at low dimensions [38–41]. This explains why even our 50 nm nanoparticles can be highly compressed with no fracture.

4. Discussion

To summarize, we find that all core–shell nanoparticles plastically deform mainly by the nucleation and propagation of dislocations. A major and unprecedented outcome is that there is a gradual change of plastic localization as a function of the SiC shell thickness. For low thickness, plasticity starts from the interface and remains confined in the Si core, then develops in both Si and SiC from the interface for intermediate values, and finally expands from the surface and almost exclusively in the SiC shell for a large thickness.

4.1. Stress concentration

To better understand our results, we find it is highly instructive to analyze the distribution of von Mises shear stresses in the nanoparticles, for strains corresponding to the first dislocation emission. Note that the comparison between different systems should remain at a qualitative level since these distributions are computed at slightly different strains. For pure Si or SiC nanoparticles, the largest stresses can be found in the region below (above) the descending (ascending) indenter (Fig. 3), with a well defined stress concentration pattern as predicted by theory of contact mechanics [42]. Maximum values in Si are approximately 1/3 of those in SiC, in agreement with the ratio between shear moduli in both materials.

For core–shell nanoparticles, except when δ = 8.8 nm, we find that there are little changes regarding the localization of the largest stresses, although different patterns of stress distributions can be distinguished. Hence the maximum stress values can be found in the SiC shell, even for low δ values like 2.5 nm and 5.0 nm. However, dislocations can first nucleate in the Si part, since the critical nucleation stress is lower than in SiC. When the shell is thick enough, the Si core is too far away from the region with high stresses, and dislocation nucleation becomes favored in the silicon carbide shell. Therefore, simple concepts from elasticity theory [42] are enough to explain the core to shell plasticity transition. It is also important

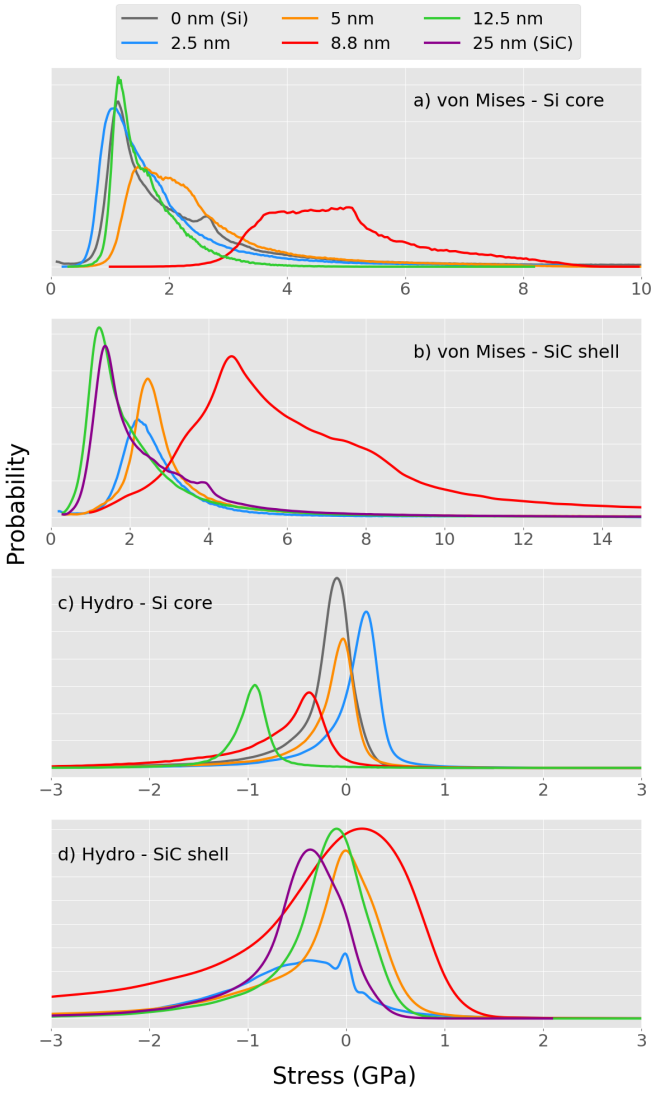

Figure 4: von Mises and hydrostatic stress distributions in the Si core and SiC shell, computed right before dislocations are nucleated, from compression tests of 50 nm nanoparticles at 5 K and a sharp interface. The curves correspond to different SiC shell thicknesses: $\delta = 0$, i.e full Si (dark grey), $\delta = 2.5$ nm (blue), $\delta = 5$ nm (orange), $\delta = 8.8$ nm (red), $\delta = 12.5$ nm (green), $\delta = 25$ nm, i.e. full SiC (magenta).

to emphasize that the configuration of the interface seems to have little influence on this result, and that a similar process is obtained regardless of temperature, and for the two investigated nanoparticle sizes.

Our simulations also revealed a puzzling feature. In fact, for a shell thickness corresponding to the transition ($\delta = 8.8$ nm), one can see in Fig. 3 that stresses are much less localized in both core and shell, compared to other δ values. In addition, it seems that high stress values are present in large regions of the SiC shell. In Fig. 4-a,b, we plot the von Mises stress distributions in both the core and the shell, for different shell thicknesses. Most curves are characterized by a seemingly log-normal shape, with a maximum around 1 GPa, and a long-range tail for high stress values. Curves for $\delta = 8.8$ nm are clearly different from the others, with a flat maximum of 3.5–5 GPa in the Si core, and a broad peak with a maximum at 4.5 GPa in the SiC shell. Moreover, the slowly decreasing tails indicate that a significant proportion of high stress values can be found, especially in the SiC shell. We also plot the hydrostatic pressure distributions in Fig. 4-c,d. For $\delta = 8.8$ nm, positive and negative values, larger than in other curves, can be found in the SiC shell. An interesting fact is that the Si core becomes almost fully compressed just when the shell thickness is equal to 8.8 nm, although it appears to be mainly in expansion for very thin shells ($\delta = 2.5$ nm)

This peculiar state for $\delta = 8.8$ nm corresponds to the transition of the plastic deformation between the shell and the core. For other thickness values, shear stress concentration occurs, leading to dislocation nucleation either in the Si core or the SiC shell. Strikingly, it seems that stress concentration mechanisms are strongly inhibited at the transition state, as though the core and the shell were exactly compensating each other. Furthermore, the geometry with $\delta = 8.8$ nm allows to attain the largest strain and stress values before dislocation nucleation. The significance of this original finding is difficult to assess. As far as we know, it has not been reported before, one possible reason being the lack of studies dedicated to mechanical properties of core–shell nanostructures. It is conceivable that an equivalent process could have been already identified from nanoindentation studies of layered materials. But it is also possible that it is unique to nanoparticles, especially if lateral deconfinement is critically needed [25].

4.2. *Influence of the interfaces*

At first sight, there are little differences of mechanical behaviors between nanoparticles with sharp or amorphous interfaces. For further analysis, the changes in von Mises stresses between the uncompressed state and the onset of dislocation formation are computed across the nanoparticles for two different cases. A slow increase of the von Mises stresses is observed for a thin SiC shell (Fig. 5-b). Sharp variations can be noticed at the interfaces and at the surface. In particular, a significant stress decrease is observed at the boundary between the Si core and the amorphous interface. We find similar features for the nanoparticle with thick shell (Fig. 5-c). Note that larger stresses are obtained for the amorphous interface compared to the sharp one, because of a slightly higher dislocation nucleation strain in the former case.

This analysis reveals differences in stress concentration between the sharp and amorphous models, especially in the vicinity of the core–shell interface. However these remain relatively small, so that the interface structure has little influence on the stress buildup in the Si core (for low δ values) or in the SiC shell (for high δ values), and on the subsequent nucleation of dislocations in these regions.

We also try to estimate the amount of plastic deformation in the amorphous interface, during compression. Unfortunately, available knowledge on plasticity in a-SiC is scarce [43], without any proven methodology to detect and monitor deformation mechanisms. In amorphous silicon, it is known that plasticity is strongly related to over-coordinated atoms [44]. By analogy,

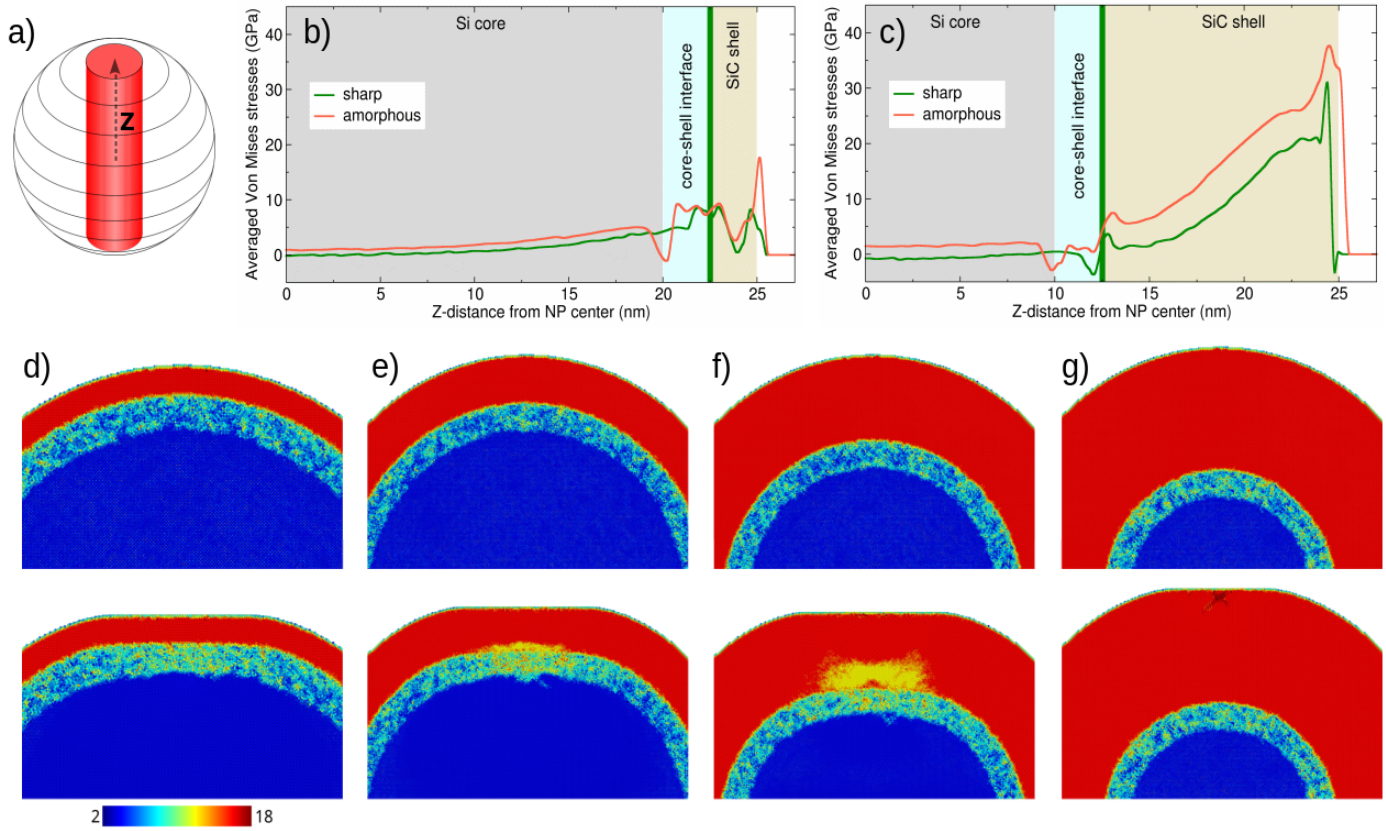

Figure 5: a–c): Change of the von Mises stresses (GPa) between the uncompressed state and the onset of dislocation nucleation for SiC shell thicknesses of a) 2.5 nm and b) 12.5 nm for both sharp (green curves) and amorphous (red curves) interfaces. The averages have been calculated for atoms inside a cylindrical region of radius 1 nm and 0.5 nm wide, which traverses the center of the nanoparticles along the compression axis (see sketch in (a)). The sharp (amorphous) interface position is marked by a thick green line (the cyan area). (d–g): cross-sectional views of the atomic coordination, computed with a cutoff of 3.2 Å, for nanoparticles with an amorphous interface and various SiC shell thicknesses (2.5 nm (d), 5 nm (e), 8.8 nm (f), 12.5 nm (g)). The top pictures show the uncompressed configurations, whereas the bottom pictures display compressed nanoparticles, just before nucleation of the first dislocations. All data reported in this figure are obtained from calculations at 5 K.

we thus investigate the evolution of atomic coordination inside the nanoparticles at 5 K (Fig. 5-d-g). An increase of coordination is clearly observed in the amorphous interface (except for δ equal to 12.5 nm), from the initial configuration to the state preceding dislocation nucleation. This might be the footprint left by plastic deformation, which would explain the relative absence of stress buildup in the interface before dislocation nucleation (Fig. 5-b). Finally, a puzzling observation is an unexpected coordination decrease in the SiC shell, in the vicinity of the interface, for thicknesses of 5 nm and 8.8 nm. We believe this might be due to a significant lateral deformation in this region, leading to a low coordination reduction. This hypothesis is supported by the fact that for both $\delta = 5$ nm and $\delta = 8.8$ nm, the nucleation of dislocation occurs at large strains, compared to the other cases ($\delta = 2.5$ nm and $\delta = 12.5$ nm). This yields high compression stresses in this region, as predicted by contact theory.

4.3. Plasticity transition between core and shell

At last, we discuss the value of the shell thickness corresponding to the plasticity transition between core and shell. One interesting question concerns its meaning and whether it could be predicted for other systems, be it with different sizes or other materials. Regarding sizes, on has to determine if δ at the transition does depend or not on the nanoparticle diameter. Alternatively, the invariant quantity could possibly be the ratio of δ over the diameters (equal to about 0.18 for the 50 nm size). To gain further insights, it seems reasonable to first try to apply the well known Hertz theory of elastic contacts. The latter suggests that the maximum shear stress is located below the indenter at a depth of approximately 0.48λ, assuming a Poisson ratio of 0.23 and a contact surface of area $\pi\lambda^2$ [42]. Assuming that the first dislocations formed in the vicinity of this specific point, plasticity could then occur in the shell or the core depending on the shell thickness. In the Hertz theory, λ has a weak $1/3$ power law dependence on the nanoparticle diameter and on the applied load. It implies that the shell thickness value associated to the transition would be constant at first approximation. Using our simulation data, we find that λ is in the range 7.9 nm–10.5 nm for the 50 nm nanoparticle, yielding a depth of 3.8 nm–5.1 nm. Thus the Hertz theory predicts a core–shell transition for a much lower shell thickness than the value found in our simulations.

Here we propose another model, based on the specific ge-

ometry of the core–shell nanoparticle and the constraints it imposes on dislocation expansion. The examination of the microstructures of plastically deformed nanoparticles in Fig. 2 suggests that for low δ, the formation of dislocations in the SiC shell is not an efficient way to relax the imposed stress because the available volume between the contact surface and the Si core is limited. If dislocations would nucleate from the contact surfaces, their expansion would be impeded by the Si core. Conversely, when $\delta = 12.5$ nm, i.e. when the Si core is smaller, these dislocations can freely expand without meeting the Si core until reaching the lateral surfaces. In this model, the plasticity transition should only depend on the ratio between δ and the nanoparticle diameter. This is confirmed here since for the 20 nm nanoparticles, we find that the transition is obtained for $\delta = 3.5$ nm, i.e. for a similar ratio of 0.18.

Our model should undoubtedly be confronted to additional works, especially including a wider set of sizes. It is also important to investigate other core–shell nanoparticles made of different materials. In particular, the fact that the SiC–Si interface appears to be a barrier to dislocations is a critical factor in the present study. In relation to this point, it would be interesting to examine the plastic deformation of hard core–soft shell SiC–Si nanoparticles.

5. Conclusion

Our investigations of the mechanical properties of Si–SiC core–shell nanoparticles, performed using molecular dynamics simulations, lead to the following results. Original plasticity mechanims and high stresses are revealed during the plastic deformation of the nanoparticles, which is fully ductile. We also find that the plastic deformation is either confined in the shell or in the core, depending essentially on the SiC shell thickness. The structure of the core–shell interface has a negligible influence on mechanical properties. We tentatively explain this phenomenon by proposing a model based on geometric constraints due to the Si core. At last, the transition between core and shell plasticity is associated to a peculiar elastic configuration, for which stress concentration appears to be suppressed.

Acknowledgements

This work was supported by ICFPAR/CEFIPRA (Indo-French Centre for the Promotion of Advanced Research) in the framework of project 5208-1. Computations have been performed using the supercomputer facilities of the Mésocentre de calcul Poitou-Charentes, and HPC resources from GENCI-CINES (Grant 2017-A0030910302).

References

[1] R. Ghosh Chaudhuri, S. Paria, Core/shell nanoparticles: Classes, properties, synthesis mechanisms, characterization, and applications, Chemical Reviews 112 (4) (2012) 2373–2433. doi:10.1021/cr100449n.

[2] M. B. Gawande, A. Goswami, T. Asefa, H. Guo, A. V. Biradar, D.-L. Peng, R. Zboril, R. S. Varma, Core-shell nanoparticles: synthesis and applications in catalysis and electrocatalysis, Chem. Soc. Rev. 44 (2015) 7540–7590.

[3] O. Kraft, P. A. Gruber, R. Mönig, D. Weygand, Plasticity in confined dimensions, Annu. Rev. Mater. Res. 40 (1) (2010) 293–317. doi:10.1146/annurev-matsci-082908-145409.

[4] J. R. Greer, J. T. D. Hosson, Plasticity in small-sized metallic systems: Intrinsic versus extrinsic size effect, Progress in Materials Science 56 (6) (2011) 654 – 724. doi:http://dx.doi.org/10.1016/j.pmatsci.2011.01.005.
URL http://www.sciencedirect.com/science/article/pii/S0079642511000065

[5] K. E. Aifantis, A. L. Kolesnikova, A. E. Romanov, Nucleation of misfit dislocations and plastic deformation in core/shell nanowires, Philosophical Magazine 87 (30) (2007) 4731–4757. doi:10.1080/14786430701589350.

[6] S. Vlassov, B. Polyakov, L. M. Dorogin, M. Vahtrus, M. Mets, M. Antsov, R. Saar, A. E. Romanov, A. Lõhmus, R. Lõhmus, Shape restoration effect in ag–SiO2 core–shell nanowires, Nanoletters 14 (9) (2014) 5201–5205. doi:10.1021/nl5019063.

[7] R. A. Fleming, M. Zou, The effects of confined core volume on the mechanical behavior of al/a-si core-shell nanostructures, Acta Mater. 128 (2017) 149–159. doi:10.1016/j.actamat.2017.02.009.

[8] J. Godet, C. Furgeaud, L. Pizzagalli, M. J. Demkowicz, Uniform tensile elongation in ausi coreshell nanowires, Extreme Mechanics Letters 8 (2016) 151 – 159. doi:http://dx.doi.org/10.1016/j.eml.2016.03.023.
URL http://www.sciencedirect.com/science/article/pii/S235243161630092X

[9] J. Rabier, L. Pizzagalli, J.-L. Demenet, Dislocations in silicon at high stress, in: L. Kubin, J. P. Hirth (Eds.), Dislocation in solids, Vol. 16, Elsevier, 2010, Ch. 93, p. 47.

[10] W. Gerberich, W. Mook, C. Perrey, C. Carter, M. Baskes, R. Mukherjee, A. Gidwani, J. Heberlein, P. McMurry, S. Girshick, Superhard silicon nanospheres, J. Mech. Phys. Solids 51 (6) (2003) 979 – 992. doi:http://dx.doi.org/10.1016/S0022-5096(03)00018-8.
URL http://www.sciencedirect.com/science/article/pii/S0022509603000188

[11] P. Valentini, W. W. Gerberich, T. Dumitrică, Phase-transition plasticity response in uniaxially compressed silicon nanospheres, Phys. Rev. Lett. 99 (2007) 175701. doi:10.1103/PhysRevLett.99.175701.
URL http://link.aps.org/doi/10.1103/PhysRevLett.99.175701

[12] A. J. Wagner, E. D. Hintsala, P. Kumar, W. W. Gerberich, K. A. Mkhoyan, Mechanisms of plasticity in near-theoretical strength sub-100 nm si nanocubes, Acta Mater. 100 (2015) 256 – 265. doi:https://doi.org/10.1016/j.actamat.2015.08.029.
URL http://www.sciencedirect.com/science/article/pii/S1359645415006060

[13] L. Yang, J. J. Bian, H. Zhang, X. R. Niu, G. F. Wang, Size-dependent deformation mechanisms in hollow silicon nanoparticles, AIP Advances 5 (7) (2015) 077162. doi:http://dx.doi.org/10.1063/1.4927509.
URL http://scitation.aip.org/content/aip/journal/adva/5/7/10.1063/1.4927509

[14] D. Kilymis, C. Gérard, J. Amodeo, U. Waghmare, L. Pizzagalli, Uniaxial compression of silicon nanoparticles: An atomistic study on the shape and size effects, Acta Mater. 158 (2018) 155–166. doi:10.1016/j.actamat.2018.07.063.

[15] M. Ollivier, L. Latu-Romain, M. Martin, S. David, A. Mantoux, E. Bano, V. Soulire, G. Ferro, T. Baron, Sisic core-shell nanowires, J. Cryst. Growth 363 (0) (2013) 158 – 163. doi:http://dx.doi.org/10.1016/j.jcrysgro.2012.10.039.
URL http://www.sciencedirect.com/science/article/pii/S0022024812007440

[16] Y.-L. Li, T. Ishigaki, Synthesis and structural characterization of core-shell si-sic composite particles by thermal plasma in-flight carburization of silicon powder, J. Ceramic Soc. of Japan 115 (11) (2007) 717.

[17] R. P. Chaukulkar, K. de Peuter, P. Stradins, S. Pylypenko, J. P. Bell, Y. Yang, S. Agarwal, Single-step plasma synthesis of carbon-coated silicon nanoparticles, ACS Applied Materials & Interfaces 6 (21) (2014) 19026–19034. doi:10.1021/am504913n.

[18] B. T. Goh, S. A. Rahman, Synthesis of nickel catalyzed si/sic coreshell nanowires by {HWCVD}, Journal of Crystal Growth 407 (2014) 25 – 30.

doi:http://dx.doi.org/10.1016/j.jcrysgro.2014.09.004.
URL http://www.sciencedirect.com/science/article/pii/S0022024814006216

[19] S. Plimpton, Fast parallel algorithms for short-range molecular dynamics, J. Comput. Phys. 117 (1) (1995) 1 – 19.

[20] Http://lammps.sandia.gov/.

[21] C. L. Kelchner, S. J. Plimpton, J. C. Hamilton, Dislocation nucleation and defect structure during surface indentation, Phys. Rev. B 58 (1998) 11085–11088. doi:10.1103/PhysRevB.58.11085.
URL http://link.aps.org/doi/10.1103/PhysRevB.58.11085

[22] S. Bel Haj Salah, C. Gerard, L. Pizzagalli, Influence of surface atomic structure on the mechanical response of aluminum nanospheres under compression, Comp. Mat. Sci. 129 (2017) 273–278. doi:10.1016/j.commatsci.2016.12.033.

[23] M. Z. Bazant, E. Kaxiras, J. F. Justo, Environment-dependent interatomic potential for bulk silicon, Phys. Rev. B 56 (14) (1997) 8542.

[24] G. Lucas, M. Bertolus, L. Pizzagalli, An environment-dependent interatomic potential for silicon carbide: calculation of bulk properties, high-pressure phases, point and extended defects, and amorphous structures, J. Phys.: Condens. Matter 22 (2010) 035802.

[25] D. Chrobak, N. Tymiak, A. Beaber, O. Ugurlu, W. Gerberich, R. Nowak, Deconfinement leads to changes in the nanoscale plasticity of silicon, Nature Nanotechnology 6 (2011) 480.

[26] R. Maaß, L. Meza, B. Gan, S. Tin, J. Greer, Ultrahigh strength of dislocation-free ni3al nanocubes, Small 8 (12) (2012) 1869–1875. doi:10.1002/smll.201102603.
URL http://dx.doi.org/10.1002/smll.201102603

[27] E. W. Wong, P. E. Sheehan, C. M. Lieber, Nanobeam mechanics: Elasticity, strength, and toughness of nanorods and nanotubes, Science 277 (5334) (1997) 1971–1975. doi:10.1126/science.277.5334.1971.

[28] J. Wang, C. Lu, Q. Wang, P. Xiao, F. Ke, Y. Bai, Y. Shen, X. Liao, H. Gao, Influence of microstructures on mechanical behaviours of SiC nanowires: a molecular dynamics study, Nanotechnology 23 (2) (2012) 025703. doi:10.1088/0957-4484/23/2/025703.

[29] G. Cheng, T.-H. Chang, Q. Qin, H. Huang, Y. Zhu, Mechanical properties of silicon carbide nanowires: Effect of size-dependent defect density, Nanoletters 14 (2) (2014) 754–758. doi:10.1021/nl404058r.

[30] F. Shimizu, S. Ogata, J. Li, Theory of shear banding in metallic glasses and molecular dynamics calculations, Materials Transactions 48 (2007) 2923.

[31] J. Guénolé, S. Brochard, J. Godet, Unexpected slip mechanism induced by the reduced dimensions in silicon nanostructures: Atomistic study, Acta Mater. 59 (2011) 7464.

[32] L. Pizzagalli, P. Beauchamp, Dislocation motion in silicon: the shuffle-glide controversy revisited, Philos. Mag. Lett. 88 (6) (2008) 421.

[33] J. P. Hirth, J. Lothe, Theory of dislocations, Wiley, New York, 1982.

[34] L. Hale, X. Zhou, J. Zimmerman, N. Moody, R. Ballarini, W. Gerberich, Phase transformations, dislocations and hardening behavior in uniaxially compressed silicon nanospheres, Comp. Mat. Sci. 50 (5) (2011) 1651 – 1660. doi:http://dx.doi.org/10.1016/j.commatsci.2010.12.023.
URL http://www.sciencedirect.com/science/article/pii/S0927025610006944

[35] L. Hale, D.-B. Zhang, X. Zhou, J. Zimmerman, N. Moody, T. Dumitrica, R. Ballarini, W. Gerberich, Dislocation morphology and nucleation within compressed si nanospheres: A molecular dynamics study, Comp. Mat. Sci. 54 (0) (2012) 280 – 286. doi:http://dx.doi.org/10.1016/j.commatsci.2011.11.004.
URL http://www.sciencedirect.com/science/article/pii/S0927025611006185

[36] P. Erhart, K. Albe, Analytical potential for atomistic simulations of silicon, carbon, and silicon carbide, Phys. Rev. B 71 (2005) 035211.

[37] X. D. Han, Y. F. Zhang, K. Zheng, X. N. Zhang, Z. Zhang, Y. J. Hao, X. Y. Guo, J. Yuan, , Z. L. Wang, Low-temperature in situ large strain plasticity of ceramic sic nanowires and its atomic-scale mechanism, Nanoletters 7 (2) (2007) 452–457. arXiv:http://dx.doi.org/10.1021/nl0627689, doi:10.1021/nl0627689.
URL http://dx.doi.org/10.1021/nl0627689

[38] K. Kendall, The impossibility of comminuting small particles by compression, Nature 272 (1978) 710.

[39] W. W. Gerberich, D. D. Stauffer, A. R. Beaber, N. I. Tymiak, A brittleness transition in silicon due to scale, J. Mater. Research 27 (2012) 552–561.

[40] F. Abed El Nabi, J. Godet, S. Brochard, L. Pizzagalli, Onset of ductility and brittleness in silicon nanowires mediated by dislocation nucleation, Modelling Simul. Mater. Sci. Eng. 23 (2) (2015) 025010.
URL http://stacks.iop.org/0965-0393/23/i=2/a=025010

[41] A. Merabet, M. Texier, C. Tromas, S. Brochard, L. Pizzagalli, L. Thilly, J. Rabier, A. Talneau, Y.-M. L. Vaillant, O. Thomas, J. Godet, Low-temperature intrinsic plasticity in silicon at small scales, Acta Mater. 161 (2018) 54–60. doi:10.1016/j.actamat.2018.09.025.

[42] K. L. Johnson, Contact mechanics, Cambridge University Press, Cambridge, 1985.

[43] I. Szlufarska, R. K. Kalia, A. Nakano, P. Vashishta, Atomistic processes during nanoindentation of amorphous silicon carbide, Appl. Phys. Lett. 86 (2) (2005) 021915. doi:10.1063/1.1849843.

[44] M. J. Demkowicz, A. S. Argon, Liquidlike atomic environments act as plasticity carriers in amorphous silicon, Phys. Rev. B 72 (24) (2005) 245205. doi:10.1103/physrevb.72.245205.